Three-Body Recombination of Cold ^{3}He–^{3}He–T$^-$ System

Ming-Ming Zhao(赵明明)[1], Li-Hang Li(李立航)[2], Bo-Wen Si(司博文)[1], Bin-Bin Wang(王彬彬)[3*], Bina Fu(傅碧娜)[4], and Yong-Chang Han(韩永昌)[1,5*]

[1]*Department of Physics, Dalian University of Technology, Dalian 116024, China*
[2]*Beijing Institute of Radio Measurement, Beijing 100854, China*
[3]*Physics and Space Science College, China West Normal University, Nanchong 637009, China*
[4]*State Key Laboratory of Molecular Reaction Dynamics, Dalian Institute of Chemical Physics, Chinese Academy of Sciences, Dalian 116023, China*
[5]*DUT-BSU Joint Institute, Dalian University of Technology, Dalian 116024, China*

(Received 5 May 2022; accepted manuscript online 29 June 2022)

The atom-atom-anion three-body recombination (TBR) and collision induced dissociation (CID) processes of the ^{3}He–^{3}He–T$^-$ system at ultracold temperatures are investigated by solving the Schrödinger equation in the adiabatic hyperspherical representation. The variations of the TBR and CID rates with the collision energies in the ultracold temperatures are obtained. It is found that the $J^{\Pi} = 1^-$ symmetry dominates the TBR and CID processes in most of the considered collision energy range. The rate of TBR (CID) into (from) the $l = 1$ anion is larger than those for the $l = 0$ and $l = 2$ anions, with the l representing the rotational quantum number of ^{3}HeT$^-$. This can be understood via the nonadiabatic couplings among the different channels.

DOI: 10.1088/0256-307X/39/8/083401

Three-body recombination (TBR) is a typical nonradiative scattering process which also serves as one of the elemental reaction mechanisms in chemistry. Compared with the nonradiative collision of two particles, TBR can lead to formation of a stable diatomic molecule, and due to the conservation of energy the third particle takes the binding energy away. Obviously, this is an exothermic reaction, and is one of the main loss mechanisms in ultracold atom systems. TBR process plays an important role in Bose–Einstein condensates, and restricts lifetime and density of Bose–Einstein condensates.[1–3] This process is also crucial in chemistry of forming weakly bound molecules, and important in atmospheric and combustion chemistry.[4] Since the process has important impact on many aspects of physics and chemistry, it has attracted great interest of many researchers.

In theoretical study, there were numbers of studies of TBR in the past two decades. Most of the earlier theoretical studies used model interaction potentials based on the assumption that the TBR rates in the zero-temperature depend on the two-body scattering length only, and the precise shape of the two-body interaction potential is unnecessary,[5] until D'Incao and Esry demonstrated both the scattering-length and the potential-energy dependencies of the TBR rate.[6] Atom-atom-atom TBR has been studied in numerous systems, such as helium atoms,[7] helium-helium-alkali-metal-atom systems,[5,8] etc. Most of the studies on TBR processes mainly focused on the neutral three-atomic boson systems, and the TBR rate in the ultracold limit could be calculated for both $J = 0$ and $J > 0$ states, where J is the total nuclear orbital angular momentum. Following the development of the hybrid trap technology, the neutrals and ions can be overlapped in the same spatial region, and hence, the study of the cold atom-ion interaction and the chemical reaction in mK regime becomes possible.[9–14] It is worth noting that in the high density environments, the chemical reactions are dominated by TBR processes.[15] In addition, the studies on the atom-atom-ion TBR processes can give insights into the kinetics of an ion immersed in a cloud of atoms, which are of importance in radiation physics,[16] gaseous radiation detectors,[17] excimer lasers and spectrometers,[18,19] etc.

When TBR process involves ions, one can expect that the TBR processes may be more obvious than that of neutral atomic ternary systems. This is because the long-range potential of atom-ion interaction (C_4/r^4) is more attractive than that of atom-atom interaction (C_6/r^6). The former is dominated by the charge induced dipole moment interaction, while the latter is dominated by the van der Waals interaction.

Currently, investigations of atom-atom-ion TBR mainly concentrated on two aspects. One is to determine the final state of the products after the TBR process, the other is to determine the relationship between the collision energy and the TBR rate.[15,20–24] Based on the assumption that the long-range atom-ion interaction C_4/r^4 governs the low energy limit of the atom-atom-ion TBR, Pérez-Ríos and Greene derived the classical energy scaling threshold law that the atom-atom-ion TBR rate K_3 and the total collision energy E should obey the relationship of $K_3 \propto E^{-3/4}$ [21] and that the molecular ion

*Corresponding authors. Email: binbinwang01@cwnu.edu.cn; ychan@dlut.edu.cn
© 2022 Chinese Physical Society and IOP Publishing Ltd

should dominate over the neutral molecule as the most formed product in the atom-atom-ion TBR process. This presumption has been verified in experiment by the TBR of ^{87}Ru+^{87}Ru+^{138}Ba$^+$ and ^{87}Ru+^{87}Ru+^{87}Ru$^+$ systems in mK regime.[15,20] Despite these achievements in experiment, the study of TBR process of neutral-neutral-ion systems has few theoretical interpretations.[25,26] For instance, the threshold law works not so perfectly in ultracold limit, since K_3 would become infinitely large as the collision energy $E \to 0$.[21] In addition, it is still challenging to perform quantum mechanical calculations of the TBR for the heavy systems such as ^{87}Ru+^{87}Ru+^{138}Ba$^+$, due to large number of atom-dimer and ion-dimer channels. Therefore, the study for the TBR of neutral-neutral-ion systems is an emerging, developing research topic with many interesting aspects worth being studied.[21,27,28]

In this work, we extend the investigation to a new system, ^{3}He–^{3}He–T$^-$. This system contains three atom-ion bound states ($l = 0, 1, 2$) with l denoting the two-body rotational quantum number for the recombination product ^{3}HeT$^-$, which is more complex than the previous reported systems[24,29,30] where the molecular ion products only contains two bound states ($l = 0, 1$). Moreover, the ^{3}He–^{3}He–T$^-$ system contains two indistinguishable fermions which is different with most of previous reported systems containing identical bosons. It can be expected that this system can provide more theoretical bases for the future research on complex collision systems. In addition, the collision induced dissociation (CID) process, which can be considered to be the reverse process of TBR, is usually applied to exploring the major mechanism of the TBR process.[31,32] Thus, we calculate not only the TBR rates K_3 but also the rates of the inverse process CID rates D_3. we have studied the dominate product after a TBR process in the ultracold limit and the dependence of the TBR rate of product on the collision energy. Furthermore, these particles are abundant in the universe, and this work is of great interest in understanding the evolution of interstellar gaseous clouds.

To describe the TBR and CID processes, we solve the time-independent Schrödinger equation (TISE) for three interacting particles using a combination of the adiabatic hyperspherical representation[33–35] and R-matrix method.[36,37] The adiabatic hyperspherical representation is constructed by the eigenfunctions and eigenvalues of the Hamiltonian with fixed-hyperradius R, and in the adiabatic hyperspherical representation, the TISE can be expressed as a set of coupled hyperradial equations. The R-matrix method is then used to extract the scattering S matrix from these coupled equations. The method used in this work has been discussed in detail in Ref. [29], and hence we just give a brief description here.

After the separation of the center-of-mass motion, three-particle systems can be described by six coordinates. For these coordinates, we use an improved version of Smith–Whiten hyperspherical coordinates $\{R, \Omega\} \equiv \{R, \theta, \phi, \alpha, \beta, \gamma\}$. R is the hyperradius, describing the overall size of the three-body system, and the hyperangles θ and ϕ describe the internal geometry of the three-body system. For the detailed definition of the hyperradius and hyperangles, one can see Ref. [36]. The remaining three Euler angles α, β, γ are used to specify the orientation of the body-fixed frame relative to the space-fixed frame.[38,39] The TISE for a three-body system interacting through the potential $V(R, \theta, \varphi)$ reads[40,41]

$$\Big[-\frac{1}{2\mu}\frac{\partial^2}{\partial R^2}+\frac{\Lambda^2+\frac{15}{4}}{2\mu R^2}+V(R,\theta,\varphi)\Big]\psi(R,\Omega)=E\psi(R,\Omega), \tag{1}$$

where Λ is the "grand angular momentum operator" and μ is the three-body reduced mass, $\mu = \sqrt{\frac{m_1 m_2 m_3}{m_1+m_2+m_3}}$, with m_i (i = 1, 2, 3) being the mass of particle i.[40,42] In the present work, we assign the tritium anion as particle 1 and the two indistinguishable fermionic helium atoms as particles 2 and 3.

The three-body interaction is expressed as a sum of the three pairwise two-body potentials,[43,44] $V(R, \theta, \varphi) = v_{\mathrm{HeT^-}}(r_{12}) + v_{\mathrm{HeHe}}(r_{23}) + v_{\mathrm{HeT^-}}(r_{31})$, where r_{ij} are the interparticle distances.[36] Note that a strict potential energy surface should include the retardation and nonadditive three-body terms. Although the retardation correction and nonadditive three-body terms are unavailable in literature for the ^{3}He–^{3}He–T$^-$ system, according to Ref. [45] and the weak polarizability characteristic for the helium atoms, we do not expect that these two terms have a significant contribution, and hence, we solely use the sum of the relevant pairwise potentials. This three-body interaction potential has been successfully applied to the calculation of several three-body collisions.[5,30,33,45] This potential supports three bound states for the molecular anion HeT$^-$, but no bound state for ^{3}He$_2$. The HeT$^-$ bound state energies and the corresponding s-wave scattering length a are summarized in Table 1, with ν and l labeling the two-body rovibrational quantum numbers.

Table 1. Two-body rovibrational energies $E_{\nu l}$, with vibrational (ν) and rotational (l) quantum numbers, and s-wave scattering lengths a calculated using the dimer potentials from Refs. [5,44].

System	(ν, l)	$E_{\nu l}$ (a.u.)	$E_{\nu l}/k_{\mathrm{B}}$ (mK)	a (a.u.)	a (Å)
^{3}HeT$^-$	(0,0)	-3.87×10^{-6}	−1222.59	−368.62	−195.07
	(0,1)	-2.58×10^{-6}	−814.24		
	(0,2)	-3.30×10^{-7}	−104.08		

To solve Eq. (1), we first solve the fixed-R adiabatic eigenvalue equation for a given symmetry J^Π, with J and Π being the total nuclear orbital momentum and parity, to determine the adiabatic eigenfunctions $\Phi_c^{J\Pi}(\Omega; R)$ and the eigenvalues $U_c(R)$,

$$\Big[\frac{\Lambda^2}{2\mu R^2}+\frac{15}{8\mu R^2}+V\Big]\Phi_c^{J\Pi}(\Omega;R)=U_c(R)\Phi_c^{J\Pi}(\Omega;R). \tag{2}$$

These angular wave functions $\Phi_c^{J\Pi}(\Omega; R)$ serve as a complete orthonormal basis set, i.e., the adiabatic hyperspherical representation, based on which the total wave function $\psi(R, \Omega)$ can be expanded with the radial wave function $F_c(R)$ as expansion coefficient,

$$\psi(R,\Omega)=\sum_c F_c(R)\Phi_c^{J\Pi}(\Omega;R), \tag{3}$$

where the quantum number c distinguishes different channels. In the adiabatic hyperspherical representation, Eq. (1) leads to a set of coupled differential equations.

$$\Big[-\frac{1}{2\mu}\frac{d^2}{dR^2}+W_c(R)\Big]F_c(R) - \frac{1}{2\mu}\sum_{c'\neq c}\Big[2P_{cc'}(R)\frac{d}{dR}+Q_{cc'}(R)\Big]F_{c'}(R) = EF_c(R), \tag{4}$$

where $W_c(R)=U_c(R)-[Q_{cc}(R)/2\mu]$ is the effective potential for the cth channel, and $P_{cc'}(R)$ and $Q_{cc'}(R)$ are nonadiabatic couplings between the cth and c'th channels. Then the scattering S matrix can be obtained from Eq. (4).

To obtain the accurate adiabatic potential and channel functions in Eq. (2), the mesh points in θ and φ should be designed carefully as described in Ref. [5]. In practice, for each given radial grid point R_i, we generate the basis splines for θ from 80 mesh points and for φ from 140 mesh points. With this setting, the eigenfunction $\Phi_c^{J\Pi}(\Omega;R_i)$ and the eigenvalues $U_c(R_i)$ can converge to at least six digits for all the 14 channels we used. A set of about 2000 radial grid points R_i are used from $R=2$ to 2000 a.u., and to accurately track the abrupt changes in the nonadiabatic couplings, the radial grid points are artificially unevenly discretized. For $R>2000$ a.u., these are extrapolated using an extrapolation procedure.[37,46]

Then, the scattering observables are obtained by solving the coupled-channel Eq. (4) using a combination of the adiabatic finite element method and the R-matrix method.[7,37,47] The TBR rate is expressed in terms of the S-matrix as[48]

$$K_3=\sum_{J,\Pi}K_3^{J\Pi}=2!\sum_{J,\Pi}\sum_i\frac{32(2J+1)\pi^2}{\mu k^4}|S_{f\leftarrow i}^{J,\Pi}|^2, \tag{5}$$

where $K_3^{J\Pi}$ is the partial recombination rate corresponding to the J^Π symmetry; i and f label the incident (three-body continuum) and recombination channels, respectively; $k=\sqrt{2\mu E}$ is the hyperradial wave number in the incident channels. $S_{f\leftarrow i}^{J,\Pi}$ is the scattering matrix element from channel i to f. With the S matrix in hand, we can also calculate the CID rate,

$$D_3=\sum_{J,\Pi}D_3^{J\Pi}=\sum_{J,\Pi}\sum_i\frac{(2J+1)\pi}{\mu_{1,23}k_{1,23}}|S_{f\leftarrow i}^{J,\Pi}|^2, \tag{6}$$

where $D_3^{J\Pi}$ is the partial dissociation rate for the J^Π symmetry. Since CID is the reverse process of TBR, the subscripts i and f in Eq. (6) correspond to the recombination (two-body) and continuum (three-body) channels, respectively, which are different from those in Eq. (5). Here, $\mu_{1,23}=m_1(m_2+m_3)/(m_1+m_2+m_3)$ is the two-body reduced mass, $k_{1,23}=\sqrt{2\mu_{1,23}(E-E_i)}$ is the two-body wave number, and E_i is the two-body binding energy as presented in Table 1.

There are three bound states in the ^{3}HeT$^-$ dimer, i.e., the three rotational states, $l=0$, 1 and 2, of the single vibrational state, $\nu=0$. Therefore, the TBR and CID processes are allowed for both the parity-favored and parity-unfavored cases for the ^{3}He–^{3}He–T$^-$ system. The $J^\Pi=1^-$ symmetry is considered to be the dominant one in the TBR and CID process, because it is the lowest available symmetry in energy for this system containing two identical fermions. Figure 1 shows the lowest fourteen adiabatic potential curves $U_c(R)$ as functions of the hyperradius R for the $J^\Pi=1^-$ symmetry. The lowest adiabatic potential curve $c=1$ at the asymptote of $R\to\infty$ corresponds to the ($l=0$) ^{3}HeT$^-$ dimer with an isolated ^{3}He atom, and the asymptotes of the curves $c=2,3$ and that of the curves $c=4,5$ correspond to the ($l=1$) ^{3}HeT$^-$ dimer and the ($l=2$) ^{3}HeT$^-$ dimer with a free ^{3}He atom, respectively. It is worth noting that, although the curves of $c=2,3$ asymptotically correspond to the same state, they actually have different orbital angular momentum l' for the relative motion between the dimer and the atom. This is also analogous for the curves of $c=4,5$. Obviously, these lowest five adiabatic potential curves are known as the recombination channels and asymptotically behave as $U_c(R)-Q_{cc}(R)/2\mu\longrightarrow E_{\nu l}+l'(l'+1)/2\mu R^2$, where $E_{\nu l}$ is the rovibrational energy of the ^{3}HeT$^-$ dimer, as shown in Table 1. The curves of higher energies $c=$ 6–14 correspond to the three-body continuum channels where all the three particles are separated from each other in the limit $R\to\infty$, and asymptotically behave as $U_c(R)-Q_{cc}(R)/2\mu\longrightarrow[\lambda(\lambda+4)+15/4]/2\mu R^2$. Here, λ is the eigenvalue of Λ^2.

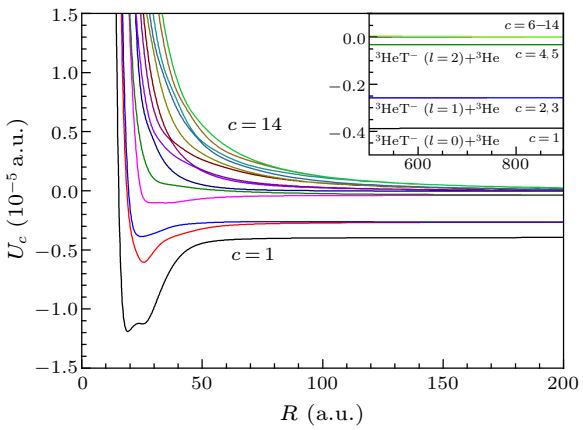

Fig. 1. The fourteen lowest adiabatic potential curves $U_c(R)$ ($c=$ 1–14) for the ^{3}He–^{3}He–T$^-$ system in the $J^\Pi=1^-$ symmetry.

In the present work, the TBR rates of the ^{3}He–^{3}He–T$^-$ system for both parity-favored and parity-unfavored cases with the total angular momentum $J<4$ are calculated. The total and partial atom-atom-anion TBR rates as functions of the collision energies for the ^{3}He–^{3}He–T$^-$ system, leading to the formation of the $l=0$, 1, 2 ^{3}HeT$^-$ anions, are shown in Figs. 2(a)–2(c), respectively. A comparison of the total TBR rates corresponding to the different dimer products is shown in Fig. 2(d). As can be seen from Figs. 2(a)–2(c), the total rates K_3 are mainly contributed from only a few partial waves. At lower collision energies, about $E<1$ mK, the red dashed curve denoting the total TBR rate K_3 coincides with the black solid one which denotes the contribution of the partial wave $J^\Pi=1^-$.

Therefore, the $J^{\Pi} = 1^-$ partial wave dominates the TBR process in this energy regime. The partial TBR rates for the system behave roughly as the prediction of the generalized Winger threshold law, i.e., $K_3^{J\Pi} \propto E^{\lambda_{\min}}$,[49] where the $\lambda_{\min}$ is the minimum value of λ allowed by the permutation symmetry. As a result, the TBR rates for this system are suppressed by decreasing the collision energy E.

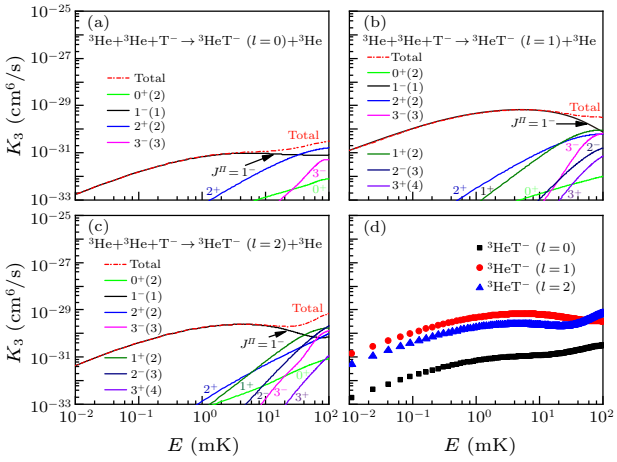

Fig. 2. Total and partial atom-atom-anion three-body recombination rates as functions of collision energy for the ^{3}He–^{3}He–T$^-$ system in the $J^{\Pi}(\lambda_{\min}) = 0^+(2), 1^-(1), 2^+(2), 3^-(3), 1^+(2), 2^-(3)$ and $3^+(4)$ symmetries (a)–(c) and a comparison of the total rates (d).

Apart from the $J^{\Pi} = 1^-$ symmetry, the other partial waves have contributions to the total TBR rate with increase of the collision energy. Taking the formation of the $l = 0$ ^{3}HeT$^-$ ion for instance, cf. Fig. 2(a), the TBR is only allowed for the parity-favored cases. The contribution from $J^{\Pi} = 2^+$ is distinguishable roughly for $E > 1$ mK, while that from $J^{\Pi} = 0^+$ is distinguishable roughly for $E > 7$ mK. However, the $J^{\Pi} = 3^-$ symmetry does not have recognizable contribution until the collision energies greater than roughly 20 mK, and in the same energy regime, the partial rate for $J^{\Pi} = 2^+$ becomes comparable to the $J^{\Pi} = 1^-$ rate.

As regards the formation of the $l = 1$ and $l = 2$ ^{3}HeT$^-$ anions shown in Figs. 2(b) and 2(c), respectively, the total TBR rates are contributed not only from the parity-favored partial waves, i.e., $J^{\Pi} = 0^+, 1^-, 2^+, 3^-$ but also from the parity-unfavored ones, i.e., $J^{\Pi} = 1^+, 2^-, 3^+$. The $J^{\Pi} = 2^-$ and 3^+ symmetries have no distinguishable contributions to the total TBR rates until $E > 10$ mK. On the contrary, the contribution from the $J^{\Pi} = 1^+$ and 2^+ symmetries are distinct for about $E > 1$ mK. Generally, in comparison of Figs. 2(a)–2(c), for the same symmetry, the corresponding partial TBR rates for the three $l = 0, 1, 2$ ^{3}HeT$^-$ anion products have similar behaviors with the variation of the collision energy, however, the total TBR rates of the formation of $l = 1$ and 2 ^{3}HeT$^-$ are larger than that of the $l = 0$ ^{3}HeT$^-$ as displayed in Fig. 2(d).

To understand the mechanism relevant to the distribution of product states for the ^{3}He–^{3}He–T$^-$ system, we simply characterize the TBR process as "jump" of flow.[30] The strength of the nonadiabatic couplings $f_{cc'}(R) = \frac{|P_{cc'}(R)|^2}{2\mu[U_c(R)-U_{c'}(R)]}$ among the adiabatic channels are shown in Fig. 3(a) as a function of hyperradius R. In Fig. 3(a) we illustrate $f_{cc'}(R)$ between the lowest three-body continuum channel $c = 6$ and all recombination channels $c = 1$–5 for the $J^{\Pi} = 1^-$ symmetry, which dominates the TBR and CID processes in most of the considered collision energy range. In addition, Fig. 3(b) shows $f_{cc'}(R)$ among those recombination channels to gain an insight into the behavior of the recombination channels.

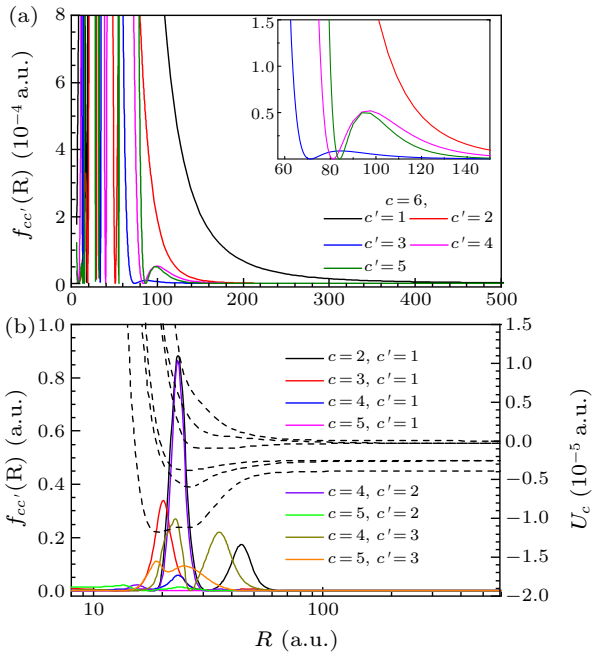

Fig. 3. (a) The nonadiabatic coupling strengths $f_{cc'}$ between the lowest incident channel ($c = 6$) and all recombination channels ($c = 1$–5) for the $J^{\Pi} = 1^-$ symmetry of the ^{3}He–^{3}He–T$^-$ system and an insert for the zoom in plot of $R = 100$ a.u. range. (b) The lowest six adiabatic potential curves U_c (black dashed curves), and the nonadiabatic coupling strengths among all the recombination channels (color curves).

As shown in Fig. 3(a), all recombination channels ($c = 1$–5) have strong couplings with the incident channel ($c = 6$) in the relatively short R range of $R < 100$ a.u., where flow of the lowest incident channel is difficult to transfer to recombination channels. The adiabatic potential energy of the lowest incident channel is several orders of magnitude larger than the collision energy considered in that R range in this work. Therefore, the large nonadiabatic couplings $f_{6c'}(R)$, ($c' = 1$–5) in this R range have little contribution to the total TBR rates, and the transition of flow from the incident to the recombination channels mainly occurs in the large R range. The $f_{61}(R)$ present relatively strong couplings in a widespread R region from roughly 100 to 400 a.u., and the coupling can be considered to be the major wide passage connecting with the incident channel ($c = 6$) and the recombination channel ($c = 1$), leading to the formation of the $l = 0$ ^{3}HeT$^-$ molecular anion. Similarly, the $l = 1$ ^{3}HeT$^-$ molecular anions are formed via the passage where the incident flow

has to "jump" into channel $c = 2$ from channel $c = 6$ via the nonadiabatic coupling $f_{62}(R)$, which locates in the region from roughly 100 to 200 a.u. The other nonadiabatic couplings are even smaller in value and shorter in range. Thus, the $f_{61}(R)$ is the most major passage connecting the incident and recombination channels, and $l = 0$ ^{3}HeT$^-$ has the most population via the direct nonadiabatic transition from the three-body continuum channel.

Based on the above comparisons among $f_{6c'}(R)$ ($c' =$ 1–5), it seems that the TBR rate for the $l = 0$ ^{3}HeT$^-$ product should dominate over the other two products ($l = 1$ and 2 ^{3}HeT$^-$). However, one should keep in mind that once a recombination channel has been populated, the flow of that channel may transfer to other recombination channels via the nonadiabatic couplings among them, and this will result in the suppression of the TBR rate for that original recombination channel.

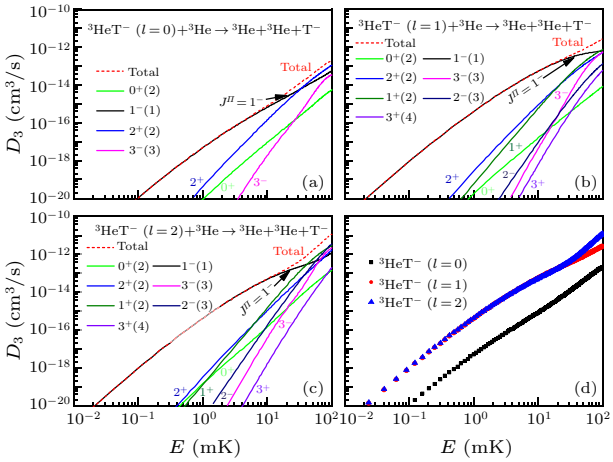

Fig. 4. Total and partial collision induced dissociation rates for the ^{3}He–^{3}He–T$^-$ system, (a) ^{3}HeT$^-$ (l=0) + ^{3}He → ^{3}He + ^{3}He + T$^-$, (b) ^{3}HeT$^-$ (l=1) + ^{3}He → ^{3}He + ^{3}He + T$^-$, and (c) ^{3}HeT$^-$ (l=2) + ^{3}He → ^{3}He + ^{3}He + T$^-$, as functions of the collision energy for the $J^\Pi(\lambda_{\min}) = 0^+(2), 1^-(1), 2^+(2), 3^-(3), 1^+(2), 2^-(3)$ and $3^+(4)$ symmetries. (d) A comparison of the total collision induced dissociation rates corresponding to different initial states.

Hence, the initially formed ^{3}HeT$^-$ population on the $l = 0$ state will further transfer to the $l = 1$ and 2 states through the pathways constructed by the couplings between the channels $c = 1$ and $v = 2$, 3, 4, 5 displayed in Fig. 3(b), which shows strong couplings within the short hyperradial range $R < 70$ a.u. This results in the fact that the rate of TBR into $l = 0$ ^{3}HeT$^-$ molecular anion is smaller than that into $l = 1$ or 2. Here, the couplings between recombination channels in the short R range will affect the flow transition process, because different from the three-body continuum channels, the recombination channels are energetically accessible in this region. In Fig. 3(b), due to the strong couplings $f_{21}(R)$ and $f_{31}(R)$, a lot of $l = 0$ ^{3}HeT$^-$ product can transfer to the $l = 1$ ^{3}HeT$^-$ product. In addition, $f_{42}(R)$ and $f_{43}(R)$ present considerable coupling strengths, which can construct passages for ^{3}HeT$^-$ to transfer from $l = 1$ to $l = 2$. However, due to the strongest coupling $f_{12}(R)$ as shown in Fig. 3(b), the rate of TBR into $l = 1$ ^{3}HeT$^-$ molecular anion is larger than that into $l = 2$ ^{3}HeT$^-$ molecular anion, thus the $l = 1$ ^{3}HeT$^-$ molecular anion is the most possible product.

The reverse process CID is analogical to the TBR process. The generalization of Wigner threshold law for the partial dissociation rate $D_3^{J\Pi}$ is proportional to $E^{\lambda_{\min}+2}$.[49] Figure 4 shows the total CID rate D_3 as well as the partial dissociation rates $D_3^{J\Pi}$ for the total angular momentum $J < 4$ as functions of the collision energy. Because CID rates are derived from exactly the same S-matrix as K_3, the behavior of the CID rates is similar to the TBR rates and we can perform the similar deduction procedure as well as similar conclusion in this reaction.

In this work, the TBR as well as the CID processes of the ^{3}He–^{3}He–T$^-$ system has been investigated using the adiabatic hyperspherical representation. Due to the relatively heavy T$^-$, the dimer anion ^{3}HeT$^-$ contains three bound states ($l = 0, 1, 2$). It is found that few partial waves have contribution to the TBR and CID processes, especially for the ^{3}HeT$^-$ ($l = 0$) dimer channel. The TBR and CID processes are dominated by the $J^\Pi = 1^-$ symmetry and generally follow the E and E^3 threshold behaviors, respectively, in the ultracold limit. Out of the three bound states ($l = 0, 1, 2$), the rates of TBR (CID) into (from) ^{3}HeT$^-$ ($l = 1$) is the most significant in the ultracold limit.

Acknowledgments. The project was supported by the National Key R&D Program of China (Grant No. 2018YFA0306503), the National Natural Science Foundation of China (Grant Nos. 21873016, 12174044, and 22103063), the International Cooperation Fund Project of DBJI (Grant No. ICR2105), and the Fundamental Research Funds for the Central Universities (Grant No. DUT21LK08).

References

[1] Chin C, Grimm R, Julienne P and Tiesinga E 2010 *Rev. Mod. Phys.* **82** 1225
[2] Myatt C J, Burt E A, Ghrist R W, Cornell E A and Wieman C E 1997 *Phys. Rev. Lett.* **78** 586
[3] Luo X Y, Zuo Y Q, Wu L N, Liu Q, Han M F, Tey M K and You L 2017 *Science* **355** 620
[4] Regal C A, Ticknor C, Bohn J L and Jin D S 2003 *Phys. Rev. Lett.* **90** 053201
[5] Suno H and Esry B D 2009 *Phys. Rev. A* **80** 062702
[6] D'Incao J P and Esry B D 2005 *Phys. Rev. Lett.* **94** 213201
[7] Suno H, Esry B D, Greene C H and Burke J P 2002 *Phys. Rev. A* **65** 042725
[8] Suno H 2017 *Phys. Rev. A* **96** 012508
[9] Zipkes C, Palzer S, Sias C and Köhl M 2010 *Nature* **464** 388
[10] Schmid S, Härter A and Denschlag J H 2010 *Phys. Rev. Lett.* **105** 133202
[11] Hall F H J, Aymar M, Boulouta-Maata N, Dulieu O and Willitsch S 2011 *Phys. Rev. Lett.* **107** 243202
[12] Grier A T, Certina M, Orucevic F and Vuletic V 2009 *Phys. Rev. Lett.* **102** 223201
[13] Ravi K, Lee S, Sharma A, Werth G and Rangwala S A 2012 *Nat. Commun.* **3** 1126
[14] Hall F H J and Willitsch S 2012 *Phys. Rev. Lett.* **109** 233202

[15] Härter A, Krükow A, Brunner A, Schnitzler W, Schnid S and Denschlag J H 2012 *Phys. Rev. Lett.* **109** 123201
[16] Neves P N B, Conde C A N and Távora L M N 2007 *Nucl. Instrum. Methods Phys. Res. Sect. A* **580** 66
[17] Neves P N B, Conde C A N and Távora L M N 2010 *Nucl. Instrum. Methods Phys. Res. Sect. A* **619** 75
[18] Jones J D C, Lister D G, Wareing D P and Twiddy J 1980 *J. Phys. B* **13** 3247
[19] Papanyan V O, Nersisyan G T, Ter-Avetisyan S A and Tittle F K 1995 *J. Phys. B* **28** 807
[20] Krükow A, Mohammadi A, Härter A, Denschlag J H, Pérez-Ríos J and Greene C H 2016 *Phys. Rev. Lett.* **116** 193201
[21] Pérez-Ríos J and Greene C H 2015 *J. Chem. Phys.* **143** 041105
[22] Wang B B 2021 *Phys. Chem. Chem. Phys.* **23** 14617
[23] Pérez-Ríos J, Ragole S, Wang J and Greene C H 2014 *J. Chem. Phys.* **140** 044307
[24] Wang B B, Jing S H and Zeng T X 2019 *J. Chem. Phys.* **150** 094301
[25] Niles F E and Robertson W W 1965 *J. Chem. Phys.* **43** 1076
[26] Mahan B H 1965 *J. Chem. Phys.* **43** 3080
[27] Krükow A, Mohammadi A, Härter A and Denschlag J H 2016 *Phys. Rev. A* **94** 030701
[28] Härter A and Denschlag J H 2014 *Contemp. Phys.* **55** 33
[29] Zhao M M, Wang B B and Han Y C 2022 *Phys. Rev. Res.* **4** 013030
[30] Wang B B, Han Y C, Gao W and Cong S L 2017 *Phys. Chem. Chem. Phys.* **19** 22926
[31] Pack R T, Walker R B and Kendrick B K 1998 *J. Chem. Phys.* **109** 6701
[32] Takayanagi T and Wada A 2002 *Chem. Phys.* **277** 313
[33] Suno H and Esry B D 2008 *Phys. Rev. A* **78** 062701
[34] Johnson B R 1980 *J. Chem. Phys.* **73** 5051
[35] Otto R, Ma J Y, Ray A W, Daluz J S, Li J, Guo H and Continetti R E 2014 *Science* **343** 396
[36] Aymar M, Greene C H and Luc-Koenig E 1996 *Rev. Mod. Phys.* **68** 1015
[37] Burke Jr. J P 1999 *PhD Dissertation* (Boulder: University of Colorado)
[38] Zhang J Y, Xu T, Ge Z W, Zhao J, Gao S B and Meng Q T 2020 *Chin. Phys. B* **29** 063101
[39] Huang J Y, Chen J, Liu S and Zhang D H 2020 *J. Phys. Chem. Lett.* **11** 8560
[40] Kendrick B K, Pack R T, Walker R B and Hayes E F 1999 *J. Chem. Phys.* **110** 6673
[41] Johnson B R 1983 *J. Chem. Phys.* **79** 1916
[42] Lepetit B, Peng Z and Kuppermann A 1990 *Chem. Phys. Lett.* **166** 572
[43] Jeziorska M, Cencek W, Patkowski K, Jeziorski B and Szalewicz K 2007 *J. Chem. Phys.* **127** 124303
[44] Casalegno M, Mella M, Morosi G and Bressanini D 2000 *J. Chem. Phys.* **112** 69
[45] Suno H and Esry B D 2010 *Phys. Rev. A* **82** 062521
[46] Nielsen E, Fedorov D V, Jensen A S and Garrido E 2001 *Phys. Rep.* **347** 373
[47] Wang K D, Zhang H X, Huang X T, Liu Y F and Sun J F 2018 *Phys. Rev. A* **97** 012703
[48] Wang Y, D'Incao J P and Esry B D 2011 *Phys. Rev. A* **83** 032703
[49] Esry K D, Greene C H and Suno H 2001 *Phys. Rev. A* **65** 010705